for submission to: 3rd International Conference on Metals and Hydrogen, 29-31 May 2018, Ghent, Belgium

SAND2017-13583C

HYDROGEN-ASSISTED FRACTURE OF ADDITIVELY MANUFACTURED AUSTENITIC STAINLESS STEELS

Chris San Marchi, Joshua D. Sugar, Dorian K. Balch
Sandia National Laboratories, Livermore CA, USA

ABSTRACT

Additive manufacturing (AM) is emerging as an important new technology that provides the ability to produce unique components and subassemblies that cannot be produced by conventional manufacturing methods. While the microstructure of AM metals is distinct from typical casting and wrought product, in some cases, the microstructures of AM metals can have features similar to welded microstructures. For component design in high-value applications, such as in aggressive environments, the effect of these unique microstructures on mechanical performance must be evaluated. This report explores hydrogen-assisted fracture of austenitic stainless steels produced by additive manufacturing. In particular, thermal hydrogen precharging is used as a surrogate for testing in high-pressure gaseous hydrogen of additively-manufactured 304L austenitic stainless steel. The fracture properties of the hydrogen-precharged additively-manufactured 304L austenitic stainless steel are reported and compared to performance of hydrogen-precharged wrought 304L and welded 304L stainless steels. The measured performance of conventional and AM material is discussed in the context of their respective microstructures with emphasis on the prognosis of AM austenitic stainless steels for service in gaseous hydrogen environments.

1.0 INTRODUCTION

Additively manufacturing technologies for metals include a diverse array of processes to build parts from powder or wire feedstocks [1]. While unique component configurations can be produced by these technologies, the materials have distinct microstructures that differ from the microstructures typically encountered in wrought, cast, welded or conventional powder metallurgy-produced materials. Subsequent manufacturing steps (such as thermal annealing, sintering or hot isostatic pressing) are often used to modify the microstructures, control defects, and mitigate residual stresses. However, additional manufacturing steps reduce the advantage of a single processing step and may reduce some beneficial characteristics of the part, such as the relatively high strength observed in the “as-built” condition, as observed for austenitic stainless steels [1,2].

In this study, the fracture behavior of additively manufactured type 304L austenitic stainless steel is evaluated with focus on materials in the as-built condition (i.e., benefiting from high strength imparted by the AM processes). In particular, hydrogen-assisted fracture is explored in the context of components exposed to gaseous hydrogen environments as in hydrogen fuel cell electric vehicles. The high-pressure hydrogen environments are simulated by thermal precharging the fracture specimens to uniform concentration of hydrogen prior to testing.

2.0 EXPERIMENTAL PROCEDURES

2.1 Materials

Rectilinear blocks were fabricated by both selective laser melting (SLM) and by direct-energy deposition (DED). An SLM block was prepared in each of two configurations, either standing up on the deposition baseplate or laying down on the baseplate; these two configurations are called a fin and boss and designated as FN and BN, respectively. Two identical builds were prepared by DED in the fin configuration, designated FL1 and FL2. The DED build is believed to have been annealed after deposition. The composition of the deposited material is provided in Table 1. All of the deposited material was nominally dense (>99% theoretical density).

The strength properties of the deposited materials were estimated from hardness measurements (Rockwell Scale A), and using data for hardness and strength for forged type 304L in Ref. [3]. These hardness-strength correlations were established to be

$$Sy = 2193 - 91.35\ HRA + 1.077\ (HRA)^2 \quad \text{eqn (1)}$$

$$Su = 1908 - 58.90\ HRA + 0.6644\ (HRA)^2 \quad \text{eqn (2)}$$

where Sy and Su are the yield strength and tensile strength respectively, and HRA is the average hardness value from Rockwell Scale A. The hardness was measured on the lateral surfaces of extracted 3-point bend specimens for fracture testing, and represent the average of 8 to 10 measurements.

Table 1. Approximate composition (wt%) of the as-built type 304L austenitic stainless steel in this study.

Fe	Cr	Ni	Mn	Si	C	N	O	S	P
Bal	18	9.8	1.4	0.6	0.01	0.05	0.04	0.004	0.013

Table 2. Hardness (Rockwell Scale A) of the tested materials and estimated strength properties using data from Ref. [3].

Designation	Hardness (HRA)	Yield Strength (MPa)	Tensile Strength (MPa)
FN	55.5	441	686
BN	52.8	372	650
FL1	51.6	348	638
FL2	48.1	292	612

2.2 Fracture Measurements

Elastic-plastic fracture tests were conducted consistent with procedures from ASTM E1820 using the 3-point bend (3PB) geometry. Rectilinear specimens were extracted from the deposits in two orientations for the SLM builds, and a single orientation for the DED builds. The L-direction is defined as the normal to the baseplate, often referred to as the build direction. The S-direction is defined as the shortest dimension of the build, except in the boss geometry where the shortest dimension is the L-direction and the T and S directions are nominally equivalent. For the BN deposit, specimens were extracted in each of the TS and SL orientations. In the FN deposit, specimens were extracted in each of the TS and LT orientations. For the DED deposits (FL), specimens were extracted only in LT orientation.

The nominal specimen geometry consisted of span (S) of 50.8 mm, thickness (B) of 6.35 mm and width (W) of 12.7 mm. The specimens were side-grooved prior to precracking, such that the reduced thickness (B_N) was about 5 mm. The machined started notch was approximately 2.5 mm deep. Precracking was conducted in K-control with an initial maximum stress intensity factor (K_{max}) of about 25 MPa $m^{1/2}$ and a normalized K-gradient (C) of -0.2 mm^{-1} (i.e., load shedding). The crack location was monitored real-time from compliance measurements at the load line; displacement was measured at the middle pin in the 3PB configuration with a standard single-arm displacement gauge. The crack was grown to a fractional crack length (a/W) of about 0.6, which corresponded to K_{max} near 18 MPa $m^{1/2}$ at the conclusion of precracking. A load ratio of 0.1 and frequency of 10 Hz were employed for all precracking.

The position of the crack during fracture testing was monitored by direct current potential difference (DCPD). A constant current of 1A was used applied at the ends of the specimen

and the voltage drop was measured across the starter notch. The voltage sense wires were approximately 2 mm on either side of the notch (i.e., 4 mm apart). The relationships from ASTM E1737 were used for determination of the crack position. Fracture testing was conducted at a constant actuator displacement rates to achieve a load line displacement of about 1 mm/h. While the rate of K increase decreased over the course of the test, the maximum loading rate was about 3 MPa $m^{1/2}$ per minute in the elastic regime and decreased by an order of magnitude once the plastic zone was fully developed, corresponding to total test length of ~3 hours. The physical crack location at the beginning and conclusion of fracture testing were measured optically and used in the fracture analysis. Standard practice for determining the J-integral fracture toughness was used to determine J_Q as the value of the J-integral at the 0.2 mm offset construction line, where the slope of the construction line was twice the flow stress. For test specimens that were hydrogen precharged, the flow stress in the hydrogen-precharged condition was used. The value of the J-integral at the 0.2 mm offset line is referred to as the fracture resistance when the material had been hydrogen-precharged to emphasize its dependence on the environment and it is denoted as J_H. The determined values of J_H were converted to units of K assuming plane strain elastic modulus of 212 MPa and are denoted K_{JH}. Single tests were performed for each condition.

2.3 Thermal Hydrogen Precharging

Thermal hydrogen precharging is commonly employed as a surrogate for testing in high-pressure gaseous hydrogen. Previous studies have shown similar loss of tensile ductility in thermally precharged austenitic stainless steels as testing in high-pressure gaseous hydrogen [4]. In this study, the 3PB test specimens were H-precharged in gaseous hydrogen at pressure of 138 MPa and temperature of 300˚C until the specimens were saturated with hydrogen (greater than 2 weeks). These precharging conditions produce an equilibrium hydrogen concentration of about 140 wt ppm. Once cooled to room temperature the hydrogen diffusion is sufficiently slow than no measurable loss of hydrogen can be detected from relatively thick specimens (greater than ~2 mm) in tens of hours. Specimens were stored at 223K (-50˚C) to mitigate hydrogen loss from the samples prior to test. Specimens were precracked after H-precharging over a period of about 8 hours.

H-precharging is known to increase the flow stress by 10-20%. Therefore, the flow stress (σ_Y) in the H-precharged condition was determined from hardness measurements after the completion of the fracture test, as described above. The estimated yield and tensile strength in the H-precharged condition for each material is provided in Table 3, while the flow stress is the defined as the average of the yield strength and tensile strength.

Table 3. Hardness (Rockwell Scale A) of the H-precharged materials and estimated strength properties using correlations hardness-strength correlations. The flow stress is the average of the yield and tensile strength.

Designation	Hardness (HRA)	Yield Strength (MPa)	Tensile Strength (MPa)	Flow stress, σ_Y (MPa)
FN	55.9	453	692	572
BN	57.5	501	718	609
FL1	51.9	353	641	497
FL2	52.8	373	650	512

3.0 RESULTS

3.1 Fracture resistance

In general, the fracture toughness (in the absence of hydrogen) could not be measured for these materials in the described geometry. With one exception, the cracks in the test specimens blunted without any significant crack advance. This observation suggests that the fracture toughness of these AM materials is greater than the maximum J-integral capacity of the specimen, which is ~250 kJ/m^2 (=$b_o\sigma_Y$/10 from ASTM E1820-09, where b_o is the remaining crack ligament). Crack extension in the H-precharged test specimens, however, was observed in all cases with typical resistance curve behavior for ductile metals as shown in Figure 1. Crack extension was relatively uniform and generally satisfied the requirements for straightness of the crack front. The fracture resistance of the relatively low strength DED materials displayed the largest fracture resistance and met the requirements for a size independent elastic-plastic fracture resistance. The higher-strength SLM materials displayed significantly lower fracture resistance; therefore, in all cases the fracture resistance is considered to be independent of the specimen size.

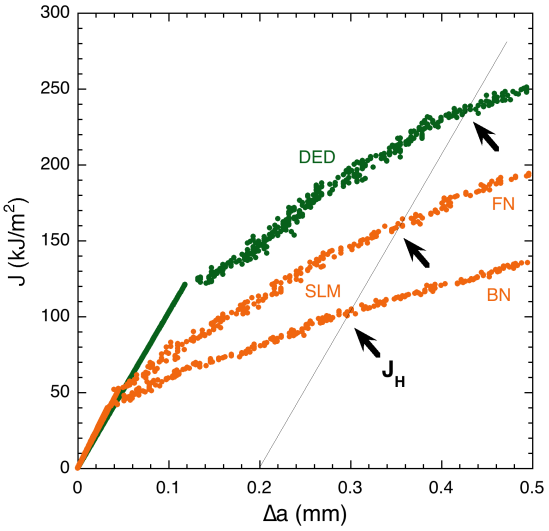

Figure 1. Example crack resistance curves for H-precharged AM type 304L austenitic stainless steels. The 0.2 mm offset construction line depends on the flow stress of each material, but for simplicity it is shown here as equivalent for all three materials.

The measured fracture resistance for both H-precharged SLM and DED type 304L is less than reported for high-quality wrought type 304L, but consistent with previous studies of welded type 304L forgings [5]. The measured values of H-precharged fracture resistance in units of stress intensity factor (K) are shown in Figure 2 as a function of yield strength, along with values from the literature for wrought type 304L [6], welded type 304L [5] and unpublished results for DED type 304L and 316L [7]. In general, the fracture resistance is lower for higher strength material and this trend is consistent with the general relationship between strength and fracture toughness. The dotted line in Figure 2 represents a notional trend line, but is not meant to be quantitative especially since the yield strength of this material was estimated from hardness measurements.

The fracture resistances are largest for cracks growing along (between) the deposited layers in the fin builds from both the DED and SLM processes (i.e., the LT orientation). While the fracture resistance for the different conditions represent individual tests and only modest differences, fracture of the TS-oriented specimens (i.e., fracture path in the S-direction) consistently displayed the lowest fracture resistance with the SL-orientation (in the BN deposit) only marginally higher. These observation suggests that interlayer boundary between successively deposited layers is more resistant to cracking than other orientations, at least in the H-precharged condition where crack extension was observed. Since each deposited layer is generally intended to melt a portion of the previous layer, the interface between these layers should represent a strong metallurgical bond, reflected in high intrinsic fracture resistance. While lack of fusion defects are often believed to populate the interfaces between deposited layers, sufficient melting of subsequent layers should mitigate these defects in high-quality deposition processes as observed here.

The relative fracture resistance values for the different orientations in the H-precharged condition suggest that cracking is promoted by characteristics other than the layered structure of the deposit. The solidification microstructure is another characteristic of these AM materials that might explain the relative fracture behavior in the presence of hydrogen. In general, solidification should induce compositional segregation perpendicular to the solidification direction, principally in columnar structures with segregation to the boundary of the columns – in welds these structures can manifest as dendrites or interdendritic structures and elongated ferrite-austenitic boundaries [5, 8]. The orientation of this solidification microstructure depends on numerous factors, but should be parallel to the primary direction of heat flow [9] or relatively parallel to the build (L) direction. Thus, local regions of nickel-lean (chromium-rich) columnar structures would be aligned normal to the successive layers (parallel to the L direction). Hydrogen-assisted fracture is sensitive to compositional segregation in wrought materials (facilitated in nickel lean regions) [10, 11] and phase boundaries in welded materials [5, 8]. Therefore, crack extension facilitated by hydrogen would be associated with columnar solidification structures when favorably oriented relative to the crack growth direction. Indeed, lower fracture resistance is observed for fracture paths perpendicular to the build direction, in particular for a fracture plane with its normal oriented orthogonal to the solidification direction represented by the TS orientation and, to a lesser extent, for a fracture plane with its normal parallel to the solidification direction represented by the SL orientation.

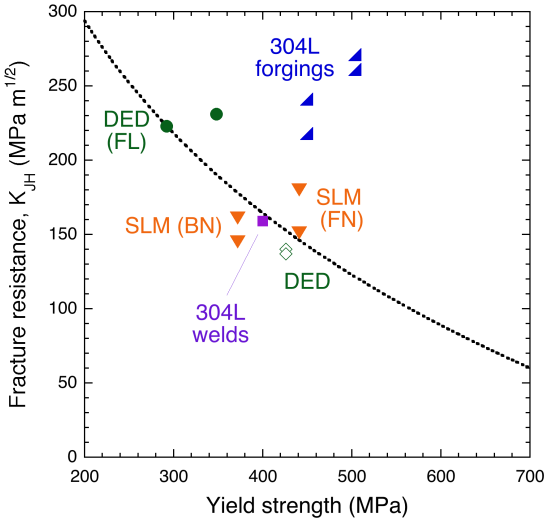

Figure 2. Fracture resistance plotted as a function of yield strength. Data also plotted for 304L forgings [6], 304L/308L gas-tungsten arc welds [5], and other DED materials (open symbols) [7]. The dotted line is an estimated trend line for the relationship between strength and fracture resistance.

3.2 Fractography

Fracture surfaces in both orientations are shown in Figure 3 for the BN deposit. These images show evidence of lack of fusion on the fracture surface that manifest as elongated crack-like structures that extend below the fracture surface. The size of these defects appears generally sub-millimeter, but can be many hundreds of microns in extent. The orientation of these elongated defects is consistent with boundaries between successive deposition layers and often non-melted (or partially melted) metal powders are apparent in these defects. The fracture resistance appears slightly greater when these defects extend in the direction of crack growth (TS, Figure 3a) compared to when the defects extend across the crack front (SL, Figure 3b). Such defects where not observed in the DED materials (Figure 4), which also showed greater fracture resistance. It is unclear if the greater fracture resistance is associated with fewer defects or with orientation (relative to deposition direction) as described in the previous section.

The rough and occasionally faceted fracture features of the H-precharged AM materials have some similarity to fracture surfaces of H-precharged wrought type 304L [6] and type 304L welds [5]. While fracture resistance appears to be greater in wrought type 304L where ferrite is absent [6], the fracture process in welded type 304L is associated with the solidification microstructure, especially presence of ferrite and ferrite boundaries [5, 8]. Whereas ferrite content on the order of 5% (by volume) is typical of gas-tungsten arc welds of austenitic stainless steel [5], ferrite is significantly lower in the DED materials (<2%) and below the detection limit of magnetic measurements in the SLM materials. Figure 3d shows flat features elongated in the nominal solidification direction, similar to features observed on fracture

surfaces of welds and attributed to ferrite [5]. It is unlikely that these features represent ferrite, but they may represent compositional segregation from the solidification process. Similarly, features in Figure 3c are suggestive of an underlying microstructure associated with solidification and suggest that H-assisted fracture in AM materials might be influenced by compositional segregation. Difficulty in asserting the exact origin of these structures can be attributed to the significantly smaller length scale that characterizes the AM microstructures compared to weld microstructures.

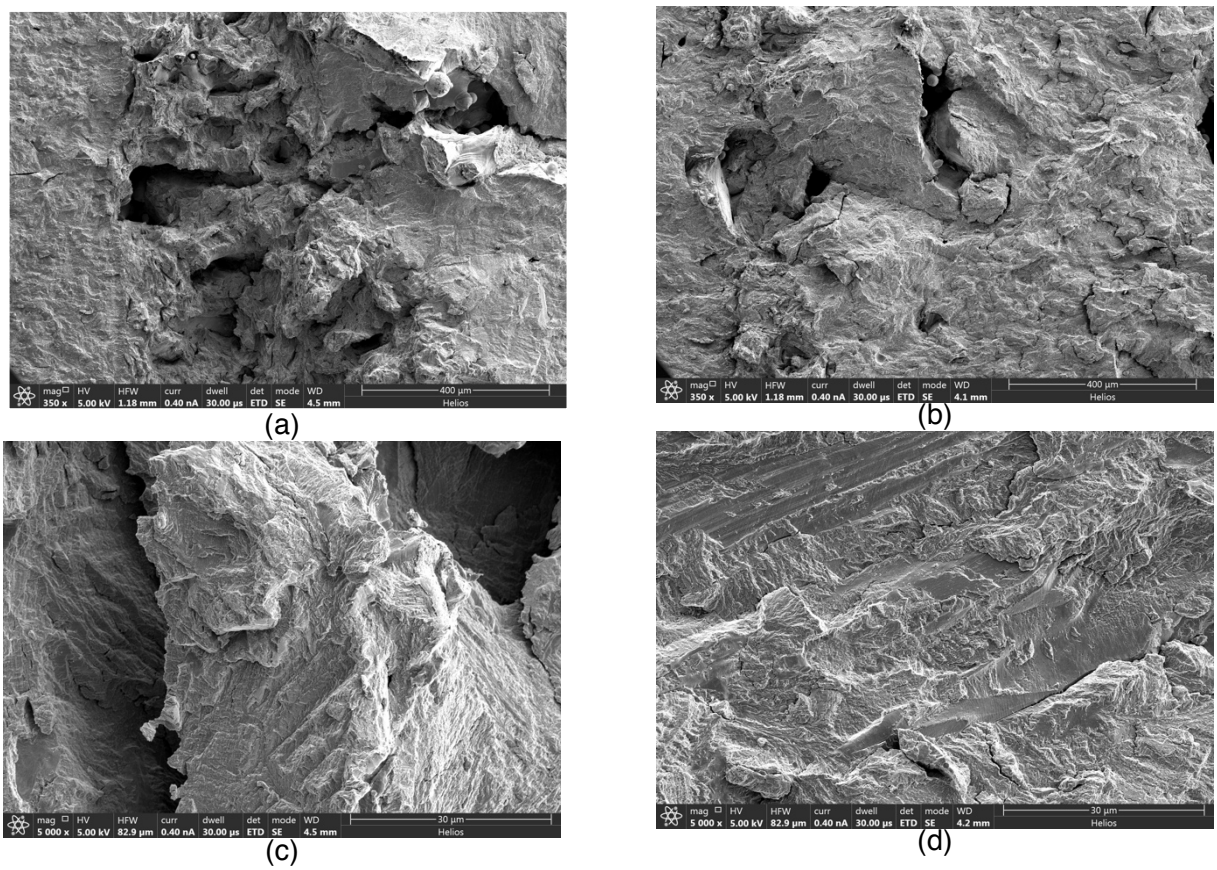

Figure 3. Fracture surfaces of BN deposit where crack extension is left to right: (a) TS orientation (L-direction is bottom to top) and (b) SL orientation (L-direction is left to right). The large crack-like defects that extend below the fracture surface are lack of fusion defects with evidence of incompletely melted powders on the surfaces of the defects. Higher magnification images are provided in (c) TS and (d) SL.

SUMMARY

Both DED and SLM type 304L austenitic stainless steels show higher strength than typical of fully annealed wrought material. The fracture toughness of these materials is sufficiently high that it cannot be measured from 3PB specimens with W on the order of 13 mm, but can be estimated as >250 kJ/m^2 (>230 MPa m$^{1/2}$). In the H-precharged condition, the fracture resistance of the SLM material is consistent with previous reports of welded type 304L (~150 MPa m$^{1/2}$) while the fracture resistance of the lower-strength DED material is significantly greater (220-230 MPa m$^{1/2}$). Despite the significantly smaller length scale in AM microstructures, the fracture surfaces show evidence of the layered and solidified microstructures similar to welds. It is hypothesized that the orientation of the solidification structures and the associated compositional segregation contribute to the relative fracture resistances measured in different orientations for the H-precharged condition. Lack of fusion defects are also apparent on the fracture surfaces, however, based on the measured values of fracture resistance, these features do not appear to play an obvious role in the fracture process in the H-precharged condition for these relatively dense AM materials.

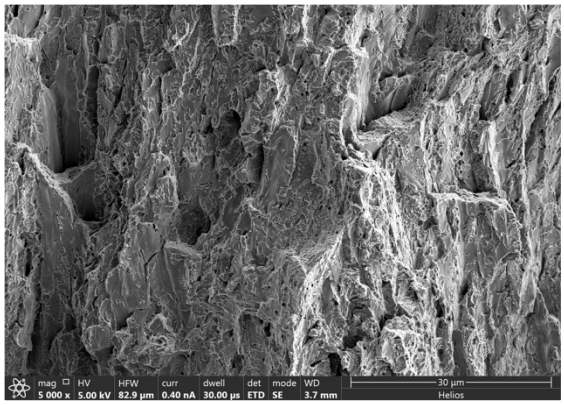

Figure 4. Fracture surface of FN deposit tested in the LT orientation; crack extension is left to right and L-direction is out of the plane of the image.

ACKNOWLEDGEMENTS

The authors wish to thank Jeff Campbell for assistance with H-precharging and Warren York for assistance with the fractography. Sandia National Laboratories is a multimission laboratory managed and operated by National Technology and Engineering Solutions of Sandia, LLC., a wholly owned subsidiary of Honeywell International, Inc., for the U.S. Department of Energy's National Nuclear Security Administration under contract DE-NA-0003525.

REFERENCES

1. T. DebRoy, H.L. Wei, J.S. Zuback, T. Mukherjee, J.W. Elmer, J.O. Milewski, A.M. Besse, A. Wilson-Heid, A. De, W. Zhang, "Additive manufacturing of metallic components – process, structure and properties", Progess Mater Sci (2017), doi: https;/doi.org/10.1016/j.pmatsci.2017.10.001.
2. Y.M. Wang, T. Voisin, J.T. McKeown, J. Ye, N.P. Calta, Z. Li, Z. Zeng, Y. Zhang, W. Chen, T.T. Roehling, R.T. Ott, M.K. Santala, P.J. Depond, M.J. Matthews, A.V. Hamza, T. Zhu, "Additively manufactured hierarchical stainless steels with high strength and ductility", Nature Materials (2017), doi: 10.1038/NMAT5021.
3. M.C. Mataya, E.L. Brown, M.P. Riendeau, "Effect of hot working on structure and strength of type 304L austenitic stainless steel", Metall Trans 21A (1990) 1969-1987.
4. C. San Marchi, T. Michler, K.A. Nibur, and B.P. Somerday, "On the physical differences between tensile testing of type 304 and 316 austenitic stainless steels with internal hydrogen and in external hydrogen", Int J Hydrogen Energy **35 (**2010) 9736-9745.
5. H.F. Jackson, K.A. Nibur, C. San Marchi, J.D. Puskar, B.P. Somerday, "Hydrogen-assisted crack propagation in 304L/308L and 21Cr-6Ni-9Mn/308L austenitic stainless steel fusion welds", Corros Sci 60 (2012) 136-144.
6. H.F. Jackson, C. San Marchi, D.K. Balch, B.P. Somerday, J. Michael, "Effects of low temperature on hydrogen-assisted crack growth in forged 304L austenitic stainless steel", Metall Mater Trans 47A (2016) 4334-4350.
7. C. San Marchi, unpublished results (2017).
8. B.P. Somerday, D.K. Balch, M. Dadfarnia, K.A. Nibur, C.H. Cadden, and P. Sofronis, "Hydrogen-assisted crack propagation in austenitic stainless steel fusion welds*",* Metall Mater Trans **40A** (2009) 2350-2362.
9. S.A. David, J.M. Vitek, M. Rappaz, L.A. Boatner, "Microstructure of stainless steel single-crystal electron beam welds", Metall Trans 21A (1990) 1753-1766.
10. T. Michler, Y. Lee, R.P. Gangloff, and J. Naumann, "Influence of macro segregation on hydrogen environment embrittlement of SUS 316L stainless steel", Int J Hydrogen Energy 34 (2009) 3201-3209.
11. C. San Marchi, K.A. Nibur, D.K. Balch, B.P. Somerday, X. Tang, G.H. Schiroky, and T. Michler, "Hydrogen-assisted fracture of austenitic stainless steels, in Effects of Hydrogen on Materials", B.P. Somerday, P. Sofronis, and R. Jones, Editors. ASM International: Materials Park OH (2009) p. 88-96.